SPC-23-007
MD-23-007

High Performance V/f control Method for Switched Reluctance Motor

Hirotaka Kato*, Jun-ichi Itoh, Takahiro Kumagai, (Nagaoka University of Technology)
Masakazu Kato, (Nagaoka Motor Development Co., Ltd.)

This paper proposes a novel V/f control method for switched reluctance motors (SRM). The proposed method does not require rotor position information. In addition, the wide operating range including the magnetic saturation region and high torque/current ratio is achieved without complicated pre-measurement or finite element analysis (FEA). The proposed V/f control consists of the following three parts and demonstrates their effectiveness with the experimental results: (A) a virtual rotor magnetic flux by controlling the zero-phase current with a PI regulator, which realizes the central part of the V/f control for the SRM, (B) the stabilization control, which is designed to be stable at all operating points since the rotor magnetic flux and inductance value change dynamically according to the operating conditions, and (C) a high torque/current ratio control by applying both $i_0 = i_q$ control and $i_d = 0$ control. In the experiment, the proposed method achieves stable operation in whole N-T regions for the tested SRM. In addition, the current RMS value is reduced by 39% at the torque of 0.05p.u. compared with no-high-efficiency control, which performs almost as the conventional drive method with the position sensor.

Keywords : Switched reluctance motor (SRM), High-efficiency, V/f control, Stabilization method, Magnetic saturation

1. Introduction

A switched reluctance motor (SRM) is composed of only an iron core and a winding without a permanent magnet using rare earth, which is cheap to manufacture. The SRM has attracted attention as a variable-speed motor for industrial applications due to the robust salient pole structure of its rotor [1][2]. The adjustable speed drive without a position sensor is expected for the SRM in order to make use of its robustness and cost-effectiveness.

Many studies for the drive method without the rotor position sensor have been examined, which uses the position dependence on the inductance or flux linkage [3-8]. In this method, first, the instantaneous value of the inductance is detected from the voltage and the current. Next, the detected inductance is converted to the rotor position information based on the look-up table or the approximation formula of the relationship between the inductance and the rotor position. However, complicated control, such as the harmonic voltage superposition [3][4] or the additional analog circuit [5][6], is required to detect the instantaneous value of the inductance accurately. In addition, the complicated pre-measurement or finite element analysis (FEA) is necessary to obtain the nonlinear magnetic model of the SRM [7][8] considering magnetic saturation.

Recently, the driving method without a rotor position sensor in the magnetic saturation region is practically essential for the miniaturization of a motor. Furthermore, the adjustment of the control parameters, such as the current amplitude, turn-on angle, and turn-off angle, are required for the design of the current and speed controllers with a high torque/current ratio, which requires pre-experiment or FEA [9][10].

This paper proposes a V/f control method for the SRM drive without the position sensor in order to solve the above problems. The V/f control does not require the rotor position information due to its control strategy based on the rotating coordinate system relative to the inverter output voltage. Therefore, the V/f control does not have the problem of the inductance detection accuracy and the conversion accuracy to the rotor position. Besides, the high-efficiency based on the maximum torque/current ratio in the field-oriented control for the SRM [11] is applied to the V/f control that achieves both simple speed control and high-efficiency drive without the rotor position sensor.

Although the principle of the proposed V/f control method for the SRM drive is based on the V/f control with the stabilization control and high-efficiency control for the PMSM [12], the following features are mainly different. (A) It is necessary to generate a virtual rotor magnetic flux corresponding to the rotor magnet magnetic flux in the PMSM. (B) It is revealed for the stabilization control gain design method, which stabilizes the SRM in the whole operating area because the rotor magnetic flux and inductance change according to the operating conditions. The experiment at the aligned position without a locked rotor test is conducted to obtain the simplified magnetic characteristic including the magnetic saturation. As a result, stabilization in the magnetic saturation region is achieved without the complicated conventional pre-measurement or FEA. (C) It is established to apply not only i_d=0 but also i_0=i_q for the high-efficiency control.

This paper is organized as follows; first, the proposed method for the above features of (A), (B), and (C) is explained; next, the usefulness of the proposed V/f control method for the SRM is demonstrated by the experimental results.

2. V/f control for switched reluctance motor

Fig.1 shows the control diagram of the proposed V/f control for the SRM. The proposed method consists of (A) zero-phase current control, (B) V/f control, and (C) high-efficiency control. The details of each control are explained and designed in the following subsections.

〈2·1〉 Zero-phase current control

The control strategy is developed based on the mathematical model in the Field-Oriented Control (FOC, i.e., vector control) for the SRM. This model has two significant parts: (i) a virtual rotor magnetic flux generated by the DC component of an excitation current, and (ii) a rotating magnetic field of the stator generated by AC component of the excitation current.

The virtual rotor flux is generated by controlling the zero-phase current with a PI regulator, which achieves the V/f control for the SRM described in Section 2.2.

〈2·2〉 V/f control

The FOC of the SRM uses the dq-axis Cartesian coordinate system with the d-axis defined as the direction of the virtual rotor flux vector and the q-axis defined as the direction 90 degrees behind the d-axis. However, the V/f control uses the γδ-axis Cartesian coordinate system with the δ-axis defined as the direction of the inverter output voltage and the γ-axis defined as the direction 90 degrees behind the δ-axis. In the V/f control for the PMSM, the torque oscillation occurs due to the resonance between the moment of inertia and the armature inductance. Then, the torque oscillation is suppressed by the damping control, which feeds back the active current i_δ to the electric angular frequency command ω^*. In the SRM, the same damping control as that for the PMSM is achieved by generating the virtual rotor flux by the zero-phase current control.

This subsection first presents the simplified state equation of the SRM. Then, the inductance considering nonlinearity is obtained from a simple approximation method. Finally, the cut-off frequency of the HPF and the damping gain are designed from the simplified state equation and the inductance.

The voltage equation and the torque equation in the γδ-axis Cartesian coordinate system are expressed as in (1) and (2), which are transformed from the equations in the dq-axis Cartesian coordinate system.

$$\begin{bmatrix} v_\gamma \\ v_\delta \\ v_0 \end{bmatrix} = R\begin{bmatrix} i_\gamma \\ i_\delta \\ i_0 \end{bmatrix} + \begin{bmatrix} L_{dc}+\frac{L_{ac}}{2}\cos(6\theta_1-2\varphi) & -\frac{L_{ac}}{2}\sin(6\theta_1-2\varphi) & \frac{L_{ac}}{\sqrt{2}}\cos(2\varphi) \\ -\frac{L_{ac}}{2}\sin(6\theta_1-2\varphi) & L_{dc}-\frac{L_{ac}}{2}\cos(6\theta_1-2\varphi) & -\frac{L_{ac}}{\sqrt{2}}\sin(2\varphi) \\ \frac{L_{ac}}{\sqrt{2}}\cos(2\varphi) & -\frac{L_{ac}}{\sqrt{2}}\sin(2\varphi) & L_{dc} \end{bmatrix} p\begin{bmatrix} i_\gamma \\ i_\delta \\ i_0 \end{bmatrix}$$
$$+2\omega_1\begin{bmatrix} -L_{ac}\sin(6\theta_1-2\varphi) & -L_{dc}-L_{ac}\cos(6\theta_1-2\varphi) & \frac{L_{ac}}{\sqrt{2}}\sin(2\varphi) \\ L_{dc}-L_{ac}\cos(6\theta_1-2\varphi) & L_{ac}\sin(6\theta_1-2\varphi) & \frac{L_{ac}}{\sqrt{2}}\cos(2\varphi) \\ 0 & 0 & 0 \end{bmatrix}\begin{bmatrix} i_\gamma \\ i_\delta \\ i_0 \end{bmatrix}$$
$$+2p(\delta)\begin{bmatrix} \frac{L_{ac}}{2}\sin(6\theta_1-2\varphi) & \frac{L_{ac}}{2}\cos(6\theta_1-2\varphi) & -\frac{L_{ac}}{\sqrt{2}}\sin(2\varphi) \\ \frac{L_{ac}}{2}\cos(6\theta_1-2\varphi) & -\frac{L_{ac}}{2}\sin(6\theta_1-2\varphi) & -\frac{L_{ac}}{\sqrt{2}}\cos(2\varphi) \\ -\frac{L_{ac}}{\sqrt{2}}\sin(2\varphi) & -\frac{L_{ac}}{\sqrt{2}}\cos(2\varphi) & 0 \end{bmatrix}\begin{bmatrix} i_\gamma \\ i_\delta \\ i_0 \end{bmatrix} \quad \cdots\cdots (1)$$

$$T = \sqrt{2}PL_{ac}i_0i_q = \sqrt{2}PL_{ac}i_0(i_\gamma\sin(2\varphi)+i_\delta\cos(2\varphi)) \quad \cdots\cdots (2)$$

where R is the winding resistance, L_{dc} and L_{ac} are the dc and ac components of the self-inductance, respectively, p is the differential operator, φ is the deviation angle between the γδ-axis Cartesian coordinate and the dq-axis Cartesian coordinate, P is the number of pole pairs, and J is the moment of inertia.

The state equation is derived by first ignoring the asynchronous term appearing as the sixth harmonic for simplification and then performing a linear approximation near the steady state in the same way as Ref. [12], and expressed as in (3),

$$p\begin{bmatrix} \Delta i_\gamma \\ \Delta i_\delta \\ \Delta i_0 \\ \Delta\omega \\ \Delta\varphi \\ \Delta\chi \end{bmatrix} = \begin{bmatrix} A_{11} & A_{12} & A_{13} & A_{14} & A_{15} & A_{16} \\ A_{21} & A_{22} & A_{23} & A_{24} & A_{25} & A_{26} \\ A_{31} & A_{32} & A_{33} & A_{34} & A_{35} & A_{36} \\ A_{41} & A_{42} & A_{43} & A_{44} & A_{45} & A_{46} \\ A_{51} & A_{52} & A_{53} & A_{54} & A_{55} & A_{56} \\ A_{61} & A_{62} & A_{63} & A_{64} & A_{65} & A_{66} \end{bmatrix}\begin{bmatrix} \Delta i_\gamma \\ \Delta i_\delta \\ \Delta i_0 \\ \Delta\omega \\ \Delta\varphi \\ \Delta\chi \end{bmatrix} + \begin{bmatrix} B_{11} & B_{12} & B_{13} & B_{14} \\ B_{21} & B_{22} & B_{23} & B_{24} \\ B_{31} & B_{32} & B_{33} & B_{34} \\ B_{41} & B_{42} & B_{43} & B_{44} \\ B_{51} & B_{52} & B_{53} & B_{54} \\ B_{61} & B_{62} & B_{63} & B_{64} \end{bmatrix}\begin{bmatrix} \Delta v_\gamma \\ \Delta v_\delta \\ \Delta v_0 \\ \Delta\omega^* \end{bmatrix} \quad (3)$$

Note that the specific formulas for each element are shown in Ref. [13].

The deviation angle φ_0 at each operating point is expressed as in (4), assuming the high-efficiency control (i_d=0, i_0=i_q) is achieved which will be detailed below (The derivation is shown in the appendix).

$$\varphi_0 = \frac{1}{2}\arctan\left(\frac{\omega_0 L_{dc}}{0.5R+\omega_0 L_{ac}}\right) \quad \cdots\cdots (4)$$

where subscript "0" of the deviation angle φ and the electric angular frequency ω, represent the steady state value. Hereinafter subscript "0" means the steady state value. The γδ-axis current i_γ, i_δ at each operating point is expressed as in (5), using the zero-phase current i_{00} at its operating point and the deviation angle defined at (4) (The derivation is shown in the appendix).

$$\begin{bmatrix} i_{\gamma 0} \\ i_{\delta 0} \end{bmatrix} = \begin{bmatrix} \frac{i_{00}}{\sqrt{2}}\sin(2\varphi_0) \\ \frac{i_{00}}{\sqrt{2}}\cos(2\varphi_0) \end{bmatrix} \quad \cdots\cdots (5)$$

The state equation of the SRM is determined by the electric angular frequency ω, the zero-phase current i_0, the motor parameters P, R, L_{dc}, L_{ac}, and the cut-off frequency of the HPF ω_c at each operating

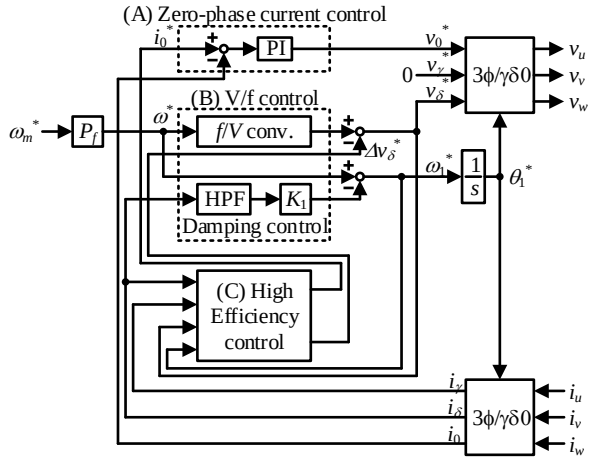

Fig. 1. V/f control method based on γδ axis.

point.

Table 1 shows test motor parameters. The test motor is an 18S/12P type SRM of 2.2 kW, 4800 rpm (=1p.u.), and 4.38 Nm (=1p.u.).

Fig.2 shows the frequency characteristics of the command speed to the motor speed under the base speed obtained from (3) and the simulation. The mathematical model presented in Ref. [11] is applied in the simulation. Fig.2 assumes i_d=0 and i_0=i_q thanks to the high efficiency control, and the figure shows the three conditions of the zero-phase current of 0.33p.u., 0.66p.u., and 1p.u. As shown in Fig.2, the calculation results by (3) are almost the same as the simulation results, i.e., the derived sixth-order equation of the state model is valid.

In order to simplify the equation, the following conditions are assumed to discuss the stability and response. It is noted that the control parameters are designed under the assumption of a steady state because the SRM is expected to apply to fans, pumps, and so on, which does not require a high torque response but only a speed control.

(i) No-load condition : $\varphi = 0$, $i_\gamma = 0$, $i_\delta = 0$

(ii) High-speed rotation condition

: $\omega_0 L_{dc}$, $\omega_0 L_{ac} >> R$, $\omega_0 L_{dc} >> K_1 i_\delta$

(iii) The mechanical time constant is sufficiently larger than the electrical time constant : $p(\Delta i_\gamma) = 0$, $p(\Delta i_\delta) = 0$, $p(\Delta i_0) = 0$

(iv) The effect of the HPF on stability is small

: $p(\Delta x) = 0$

The natural angular frequency ω_n and the damping factor ζ are calculated from the characteristic equation of the second-order system, which is derived by approximating the derived sixth-order state equation expressed as in (1) as a second-order system from the assumption of from (i) to (iv), and described as in (6),

$$[\omega_n, \varsigma] = \left[\frac{2P\Phi_r}{\sqrt{JL_{dc}}}, \frac{2}{P}\sqrt{\frac{J}{L_{dc}}}K_1 \right] \quad \text{..... (6)}$$

where K_1 is the damping gain, Φ_r is the virtual rotor flux,

$$\Phi_r = \frac{L_{ac}}{\sqrt{2}} i_0 \quad \text{..... (7)}$$

where i_0 is the zero-phase current. As shown in (6), the damping factor ζ is the function of the feedback gain K_1. In other words, the proposed V/f control is stabilized by setting K_1 appropriately. Comparing the natural angular frequency and the damping factor in the IPMSM [12], the rotor magnet magnetic flux corresponds to the virtual rotor magnetic flux in considering the difference of the coefficient by the transformation methods which are the absolute transformation and the reactive transformation. Note that (6) is applied the absolute transformation. In addition, the q-axis inductance corresponds to the dc components of the self-inductance L_{dc}.

The cut-off frequency of the HPF for the stabilization control is set to 1/20 of the natural frequency ω_n [14][15]. Note that ω_n is changed by the zero-phase current, as shown in (6). Therefore, the cut-off frequency of the HPF is designed from the lower-limit value of i_0 (i_{0Low}) in order to be always lowered enough compared with the ω_n, even when i_0 is changed. i_{0Low} is defined as 1/10 of i_0

Table 1 Motor parameters of test motor

Rated power	2.2kW
Base speed(1p.u.), Max. speed	4800rpm, 7200rpm
Max. torque(1p.u.)	4.38Nm
DC voltage	300V
Poles	Stator:18, Rotor:12
Inertia	62.3×10^{-4}kgm^2
Resistance	0.45Ω
DC inductance	7.82mH
AC inductance	5.19mH
Rated current(1p.u.)	7.7A(i_{0Max}, i_{qMax})

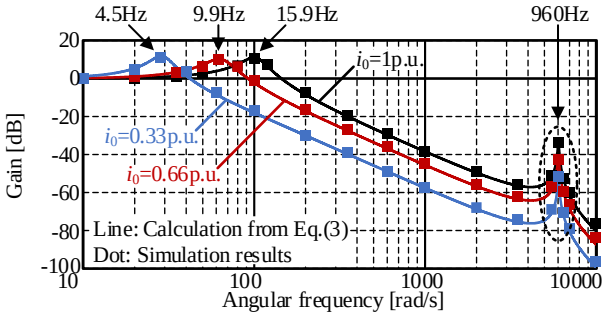

Fig. 2. Frequency characteristics of speed command to motor speed at base speed (0.6p.u.) with i_0=i_q, i_d=0.

in order that the phase-current is always bigger than zero, even under the light loading condition. The cut-off frequency of the HPF ω_c is expressed as in (8).

$$\omega_c = \frac{\omega_n}{20} = \frac{1}{20}\frac{2P}{\sqrt{JL_{dc}}}\frac{L_{ac}}{\sqrt{2}} i_{0Low} = \frac{1}{20}\frac{2P}{\sqrt{JL_{dc}}}\frac{L_{ac}}{\sqrt{2}}\frac{i_{0Low}}{10} \quad \text{..... (8)}$$

The cut-off frequency of the HPF is determined by motor parameters P, L_{dc}, L_{ac}, and rated zero-phase current i_0.

The self-inductance L_{dc} and L_{ac} are necessary to obtain the controller parameters. This paper adopts a simple approximation method for the inductance to consider the magnetic saturation. The magnetic characteristic at the aligned position, which has the strongest nonlinearity, is acquired from the measured current when one pulse voltage is injected. The magnetic characteristic at the aligned position is expressed as in (9), using a polynomial approximation.

$$\Phi_a = \sum_{n=1}^{N} k_n i^n \quad \text{..... (9)}$$

where k_n is each coefficient of the polynomial approximation and N is the maximum order of the polynomial approximation. N has to be in relatively high order in order for the magnetic characteristic at the aligned position to be expressed accurately. N is determined by the approximation accuracy of the magnetization curve and is 10 in this paper. Since the maximum current value, I_{max}, is expressed as twice the zero-phase current i_{00} (I_{max}=2*i_{00}), assuming the high-efficiency control (i_d=0, i_0=i_q) is achieved as detailed in detail below, the average inductance at the aligned position is expressed as in (10),

$$L_a(i_{00}) = \frac{\Phi_a(I_{Max})}{I_{Max}} = \sum_{n=1}^{N} k_n {I_{Max}}^{n-1} = \sum_{n=1}^{N} k_n \left(2i_{00}\right)^{n-1} \quad \text{..... (10)}$$

DC and AC components of self-inductance considering the magnetic saturation L_{dc}, L_{ac} is expressed from the inductance at the aligned and unaligned position L_a, L_u as in (11),

$$[L_{ac}(i_{00}),\ L_{ac}(i_{00})]=\left[\frac{L_a(i_{00})-L_u}{2},\ \frac{L_a(i_{00})+L_u}{2}\right] \quad \text{..... (11)}$$

Fig.3 shows the loot locus of the sixth-order state equation when the damping gain K_1 is increased at the rated load and the base speed. Note that No. 1 to No.6 are the characteristic roots of the sixth-order state equation. As shown in Fig.3, poles named No.1 and 2 moves toward the right-half plane as K_1 decreases. On the other hand, No.3 and 4 moves toward the right-half plane as K_1 increases.

From Fig.3, the following three variables are defined:

(i) The lower-limit value of K_1, K_{1Low}

: The SRM is at the stability limit caused by No.1 and 2, when K_1=K_{1Low}.

(ii) The most stable value of K_1, $K_{1Stb.}$

: The dominant poles of the SRM have the farthest from the imaginary axis when K_1= $K_{1Stb.}$. In this condition, the real part of poles No. 1, 2, 3, and 4 matches.

(iii) The upper-limit value of K_1, K_{1Up}

: The SRM is at the stability limit caused by No.3 and 4 when K_1=K_{1Up}.

Note that suppression of the overshoot of the motor rotation speed is achieved in the same way as Refs. [14][15].

Fig.4 shows the relationship between the zero-phase current and the K_{1Low}, $K_{1Stb.}$, and K_{1Up}. $K_{1Stb.}$ is changed by the zero-phase current. The transient response is improved when K_1 is adjusted to $K_{Stb.}$ according the zero-phase current. However, the control system would be complex. Therefore, K_1 is set to be within the stable value in all conditions and the closest value with $K_{Stb.}$.

Fig.5 shows the flowchart of the design of the damping gain K_1. The input parameters are the moment of inertia J, the number of pole pairs P, and rated zero-phase current i_0. First, the inductance at the unaligned position and the resistance, which is independent of the current, is measured. Second, the i-Φ_a(ι) characteristic at the aligned position is derived with the approximation, as shown in (9). This characteristic is acquired by the injection of the one pulse voltage. This measurement is relatively easy compared to the complicated pre-measurement, including the locked rotor test or the FEA. Third, the cut-off frequency of the HPF is calculated from the lower-limit value of the zero-phase current i_{0LOW} and (8). Then, the lower-limit value K_{1Low}, most stable value $K_{1Stb.}$, and upper-limit value K_{1Up} of the damping gain are calculated in the different zero-phase current from the lower-limit value i_{0LOW} to the rated value i_{0Max}. Finally, K_1 to stabilize the SRM is adopted.

〈2·3〉 High-efficiency control

Fig.6 shows the control diagram of the high-efficiency control for the SRM. The high-efficiency control improves the torque/current ratio by adjusting the inverter output voltage. The following conditions achieve the maximum torque/current ratio in the SRM.

$$i_0=\sqrt{2}i_q \quad \text{..... (12)}$$

$$i_d=0 \quad \text{..... (13)}$$

Note that the zero-phase current is larger than AC current amplitude because this paper uses the asymmetric half-bridge converter for the unipolar driving, and negative current does not flow ($\sqrt{2}$ in (12) is the coefficient of the park transformation.). Therefore, it is necessary to apply not only i_d=0 but also i_0=i_q for the high-efficiency control.

First, the i_0=i_q control is explained. i_q is equal to the AC current amplitude I_{ac} when i_0=0. Thus, i_0 should be controlled to I_{ac}, not to flow the negative current. The command value of zero-phase current control is expressed as (14).

$$i_0^*=\sqrt{2}i_q=\sqrt{2}I_{ac}=\sqrt{2}\sqrt{i_\gamma^{\,2}+i_\delta^{\,2}} \quad \text{..... (14)}$$

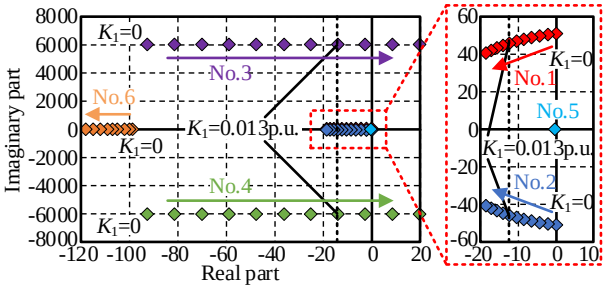

Fig. 3. Loot locus of sixth-order state equation when damping gain K_1 is increased at base speed (0.6p.u.) with i_0=i_q, i_d=0.

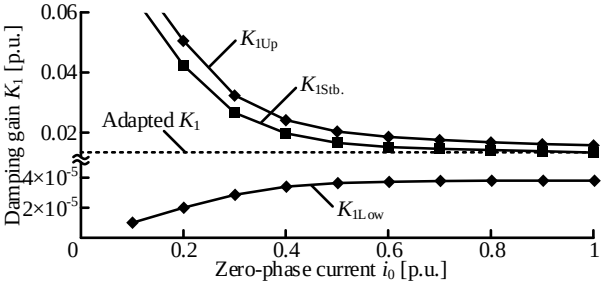

Fig. 4. Relationship between zero-phase current and damping gain K_1.

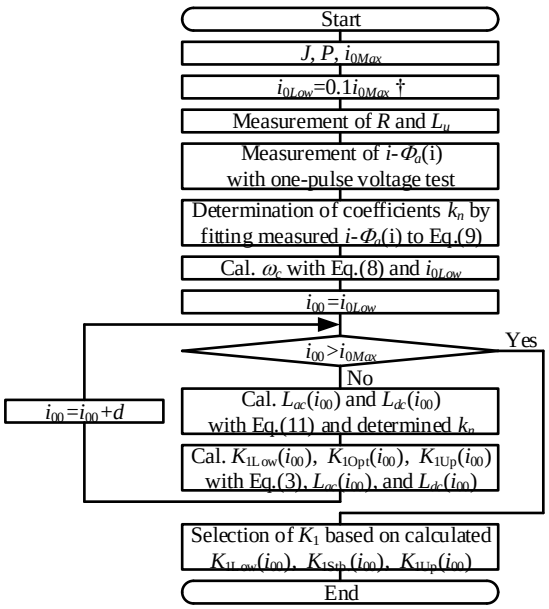

† The lower-limit value i_{0Low} is set the maximum value i_{0Max} by considering the detection accuracy of current sensor and the effect of deadtime

Fig. 5. Design flow of the damping gain K_1

where i_γ and i_δ are the γ-axis and δ-axis current, respectively.

Next, the i_d=0 control is explained. The i_d=0 control is achieved indirectly in the γδ-axis coordinate by focusing on the reactive power of the SRM. In the dq-axis coordinate, the reactive power Q_{dq} input into the SRM is expressed as in (15).

$$Q_{dq} = v_q i_d - v_d i_q = 2\omega\left\{L_{dc}(i_d^{\,2} + i_q^{\,2}) + L_{ac} i_0 i_d / \sqrt{2}\right\} \quad \text{..... (15)}$$

where v_d and v_q are the d-axis and q-axis current respectively. The reactive power Q_{dq} under the condition of i_d=0 is expressed as in (16),

$$Q_{dq} = 2\omega L_{dc} i_q^{\,2} = 2\omega L_{dc} I_{ac}^{\,2} = 2\omega L_{dc}(i_\gamma^{\,2} + i_\delta^{\,2}) \quad \text{..... (16)}$$

On the other hand, in the γδ-axis coordinate, the reactive power $Q_{\gamma\delta}$ is expressed as in (17),

$$Q_{\gamma\delta} = v_\delta i_\gamma \quad \text{..... (17)}$$

Therefore, the v_δ should be adjusted by the P controller in order to match the reactive power $Q_{\gamma\delta}$ calculated by (17) to the reactive power Q_{dq} calculated by (16). As shown in Fig.6, the value calculated by (14) is applied as the command value for zero-phase current control for the i_0=i_q control. On the other hand, the deviation between (16) and (17) is regulated to be zero by adjusting the v_δ with the P controller for the i_d=0 control. Note that the LPF in the second stage of the P controller shown in Fig.2 is to achieve the i_d=0 control at a steady state by reducing the gain for high frequencies [15]. In addition, a limit is provided in order to prevent overcompensation.

3. Experimental results

The load side servo outputs the arbitrary constant torque. In addition, the instantaneous torque is measured by a high-response torque meter (UTMII-10 Nm, 1 kHz bandwidth, UNIPULSE). The V/f ratio is set so that the modulation index is 1 at the base speed (1p.u.).

Fig. 7 shows the effect of stabilization control. Speed and torque are 1p.u. There is no oscillation in the U-phase current and torque when the stabilization control is active. These results indicate the effectiveness of the stabilization control.

Fig.8 shows the experiment results that starting is achieved with 1p.u. torque from zero-speed to base speed. Note that the motor is accelerated by the boost voltage after generating the zero-phase current of the rated value i_{0Max} by the PI regulator at the stop condition. As a result, the acceleration with the rated torque (i.e. rated acceleration time) is achieved. Although the step-out does not occur, the torque is oscillating because the torque changes rapidly at the start and end of the acceleration. This is because each control system is designed under a steady state. The design of the control system, consider including the transient response, will be future work.

Fig.9 shows the speed and torque curves. The proposed method achieves drive at 1p.u. torque and at from 0.1p.u. to 1p.u. speed. In addition, the proposed method drives with the rated power from 1p.u. to 1.5p.u. speed. Note that the rated torque is not output at 0.1p.u. speed or lower because of the output voltage error due to the dead time.

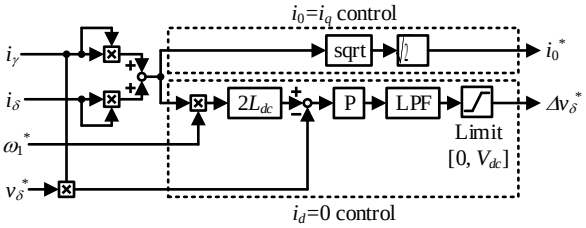

Fig. 6. High efficiency control method

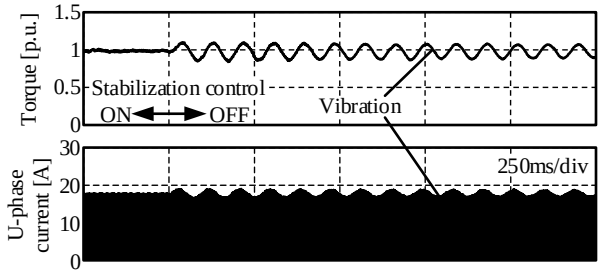

Fig. 7. Effect on the stabilization control.

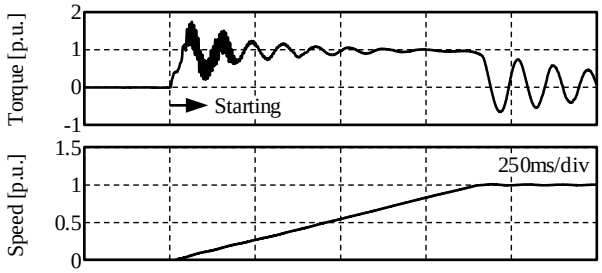

Fig. 8. Starting at i_0, i_q=1.0p.u.

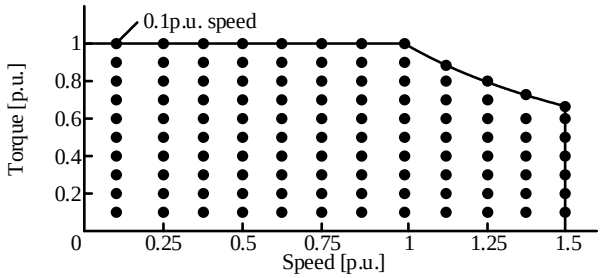

Fig. 9. Speed and torque curves

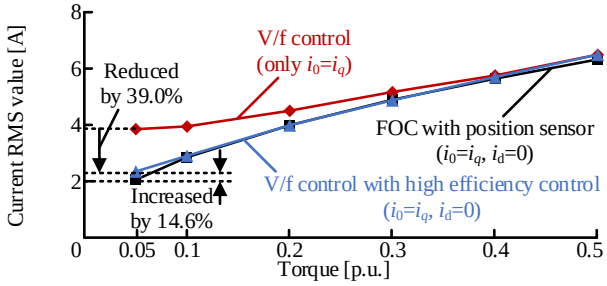

Fig. 10. Effect of high-efficiency control (0.1p.u. speed).

Fig.10 shows the effect of the high-efficiency control at the speed of 0.1 p.u. The current of the proposed method (V/f control with i_0=i_q and i_d=0) is compared with that of the FOC with i_0=i_q and i_d=0 and that of V/f control with only i_0=i_q. The current RMS value is reduced by 39.0% compared with the only i_0=i_q control at the torque of 0.05 p.u. On the other hand, the current RMS value is increased by 14.6% compared with the FOC with the position sensor. However, the increase in the current RMS value is small at large torque. Therefore, the proposed drive without the position sensor brings out the same performance as the drive with the position sensor.

4. Conclusions

This paper proposed a high-performance control method based on a V/f control for the SRM. The following three parts are proposed and demonstrated their effectiveness: (A) generating the virtual rotor magnetic flux by controlling the zero-phase current, which realizes the V/f control for the SRM, (B) designing the stabilization control gain which makes the SRM stable at all operating points when the motor parameter changes dynamically, and (C) achieving the high-efficiency drive by applying both the i_0 = i_q control and i_d = 0 control. Stable operation in all N-T regions is demonstrated in the experiment with the tested SRM. As the result, the current RMS value is reduced by 39% at 0.05p.u. torque compared with the case of no-high efficiency control, which is almost the same performance as driving with the position sensor.

References

(1) T. Kosaka, A. Kume, H. Wakayama, and N. Matsui: “Development of high torque density and efficiency switched reluctance motor with 0.1mm short airgap”, 2007 European Conference on Power Elec. App., pp. 1-9 (2007)
(2) H. Yamai, Y. Sawada, and K. Ohyama: “Applying Switched Reluctance Motor to Oil Hydraulic Pump Use”, IEEJ Trans. on Ind. App., Vol.123, No.2, pp.96-104 (2003)
(3) K.-W. Hu, Y.-Y. Chen, and C.-M. Liaw: “A reversible position sensorless controlled switched-reluctance motor drive with adaptive and intuitive commutation tunings”, IEEE Trans. Power Electron., Vol.30, No.7, pp.3781-3793 (2015)
(4) K. Ha, R.Y. Kim, and R. Krishnan: “Position estimation in switched reluctance motor drive using the first switching harmonics through fourier series”, IEEE Trans. Ind. Electron., Vol.58, No.12, pp.5352–5360 (2011)
(5) G.G. Lopez, P.C. Kjaer, and T.J.E. Miller: “A new sensorless method for switched reluctance motor drives”, IEEE Trans. Ind. App., Vol.34, No.4, pp.832–840 (1998)
(6) S. Sumita, K. Deguchi, and Y. Iwaji: “Position Sensorless Control Method for SRM Using Analog Circuit of Type-1 Control System”, IEEJ Trans. Ind. App., Vol.137, No. 8, pp.612-621 (2017)
(7) T. Kosaka, K. Ochiai, and N. Matsui: “Sensorless Control of SRM using Magnetizing Curves”, IEEJ Trans. Ind. App., Vol.120, No.2, pp.216-222 (2000)
(8) T. Kosaka, Y. Nabeya, K. Ohyama, and N. Matsui: “Position Sensorless Drive of SRM Mounted on Hydraulic Pump Unit”, IEEJ Trans. Ind. App., Vol.123, No.2, pp.103-111 (2003)
(9) K.M. Rahman, B. Fahimi, G. Suresh, A.V. Rajarathnam, and M. Ehsani: “Advantages of Switched Reluctance Motor Applications to EV and HEV: Design and Control Issues”, IEEE Trans. on Ind. App., Vol.36, No.1, pp.111–121 (2000)
(10) I. Husain and S.A. Hossain: “Modeling, Simulation, and Control of Switched Reluctance Motor Drives”, IEEE Trans. on Ind. Electron., Vol.52, No.6, pp.1625–1634 (2005)
(11) N. Nakao and K. Akatsu: “Vector Control Specialized for Switched Reluctance Motor Drives”, IEEE Trans. on Ind. App., Vol.134, No.12, pp.1006–1015 (2014)
(12) J. Itoh, J. Toyosaki, and H. Ohsawa: “High performance V/f control method for PM Motor”, Vol.122, No.3, pp.235-259 (2002)
(13) T. Kumagai, J. Itoh, and M. Kato: “V/f Control for Switched Reluctance Motor”, 2022 IEEE Energy Conversion Congress and Exposition (ECCE), pp. 1-6 (2022)
(14) T. Toi, M. Kato, and J. Itoh: “Parameter Design Considering Loot Locus for Damping Control Based on V/f control of IPMSM”, 2016 Kansai-section Joint Convention of Institutes of Electrical Engineering, No. G4-22 (2016)
(15) T. Toi, K. Nishizawa, and J. Itoh: "Stabilization Method for IPMSM with Long Electrical Time Constant Using Equivalent Resistance Gain Based on V/f Control", IEEJ Trans. on Ind. App., Vol. 8, No. 4, pp. 592-599 (2019)

Appendix

The relationship between the dq-axis current and the dq-axis current is expressed as in (A41),

$$\begin{bmatrix} i_\gamma \\ i_\delta \\ i_0 \end{bmatrix} = \begin{bmatrix} \cos(2\varphi) & \sin(2\varphi) & 0 \\ -\sin(2\varphi) & \cos(2\varphi) & 0 \\ 0 & 0 & 1 \end{bmatrix} \begin{bmatrix} i_d \\ i_q \\ i_0 \end{bmatrix} \quad \text{.....(A-41)}$$

Equation (5) is derived, substituting (12) and (13) into (A-41) under the assumption that high-efficiency control is achieved. The simplified the δ-axis voltage is derived by ignoring the asynchronous term appearing as the sixth harmonic for simplification in the steady state, which is expressed as in (A-42),

$$\begin{aligned} v_\delta &= Ri_\delta + 2\omega\left(L_{dc} i_\gamma + \frac{L_{ac}}{\sqrt{2}} \cos(2\varphi) i_0 \right) \\ &= R\frac{i_0}{\sqrt{2}}\cos(2\varphi) + 2\omega\frac{i_0}{\sqrt{2}}\left(L_{dc}\sin(2\varphi) + L_{ac}\cos(2\varphi) \right) \end{aligned} \quad \text{(A-42)}$$

Assuming that the reactive power Q_{dq} in the dq-axis expressed as expressed in (16) is equal to that in the γδ-axis as in (17), (A43) is obtained from (14) and (5).

$$\omega L_{dc} {i_0}^2 = v_\delta \frac{i_0}{\sqrt{2}} \sin(2\varphi) \quad \text{.....(A-43)}$$

Substituting (A-42) into (A-43), the deviation angle between the dq-axis and the γδ-axis is expressed as

$$\frac{\omega L_{dc}}{0.5R + \omega L_{ac}} = \frac{\sin(2\varphi)}{\cos(2\varphi)} = \tan(2\varphi) \quad \text{.....(A-44)}$$

Thus, (4) is derived by solving (A-44) for φ.